Ammonium and nitrite oxidation at nanomolar oxygen concentrations in oxygen minimum zone waters

Laura A. Bristow[a,1,2], Tage Dalsgaard[b], Laura Tiano[c], Daniel B. Mills[a], Anthony D. Bertagnolli[d], Jody J. Wright[e], Steven J. Hallam[e], Osvaldo Ulloa[d], Donald E. Canfield[a], Niels Peter Revsbech[c], and Bo Thamdrup[a]

[a]Nordic Center for Earth Evolution, Department of Biology, University of Southern Denmark, 5230 Odense M, Denmark; [b]Department of Bioscience, Arctic Research Centre, Aarhus University, 8000 Aarhus C, Denmark; [c]Department of Bioscience, Microbiology, Aarhus University, 8000 Aarhus C, Denmark; [d]Departmento de Oceanografía and Instituto Milenio de Oceanografía, Universidad de Concepción, 4070386 Concepcion, Chile; and [e]Department of Microbiology and Immunology, University of British Columbia, Vancouver, BC, Canada V6T 1Z3

Edited by David M. Karl, University of Hawaii, Honolulu, HI, and approved July 26, 2016 (received for review January 9, 2016)

A major percentage of fixed nitrogen (N) loss in the oceans occurs within nitrite-rich oxygen minimum zones (OMZs) via denitrification and anammox. It remains unclear to what extent ammonium and nitrite oxidation co-occur, either supplying or competing for substrates involved in nitrogen loss in the OMZ core. Assessment of the oxygen (O_2) sensitivity of these processes down to the O_2 concentrations present in the OMZ core (<10 nmol·L^{-1}) is therefore essential for understanding and modeling nitrogen loss in OMZs. We determined rates of ammonium and nitrite oxidation in the seasonal OMZ off Concepcion, Chile at manipulated O_2 levels between 5 nmol·L^{-1} and 20 μmol·L^{-1}. Rates of both processes were detectable in the low nanomolar range (5–33 nmol·L^{-1} O_2), but demonstrated a strong dependence on O_2 concentrations with apparent half-saturation constants (K_ms) of 333 ± 130 nmol·L^{-1} O_2 for ammonium oxidation and 778 ± 168 nmol·L^{-1} O_2 for nitrite oxidation assuming one-component Michaelis–Menten kinetics. Nitrite oxidation rates, however, were better described with a two-component Michaelis–Menten model, indicating a high-affinity component with a K_m of just a few nanomolar. As the communities of ammonium and nitrite oxidizers were similar to other OMZs, these kinetics should apply across OMZ systems. The high O_2 affinities imply that ammonium and nitrite oxidation can occur within the OMZ core whenever O_2 is supplied, for example, by episodic intrusions. These processes therefore compete with anammox and denitrification for ammonium and nitrite, thereby exerting an important control over nitrogen loss.

oxygen | ammonium oxidation | nitrite oxidation | OMZ | kinetics

Oxygen (O_2) is a key factor regulating biogeochemical cycling in the marine environment (1). Although the vast majority of the ocean remains well oxygenated, subsurface regions of extreme oxygen depletion can persist along eastern boundaries of the world's ocean basins. These regions are known as oxygen minimum zones (OMZs) and are located within the eastern tropical North and South Pacific, the Arabian Sea, and off the coast of Namibia, where oxygen depletion results from poor ventilation and a high export of organic matter from productive surface waters, generating high rates of subsurface oxygen consumption (2, 3).

Oceanic waters characterized by oxygen-deficient conditions (<4.5 μmol·L^{-1} O_2) account for <0.1% of total ocean volume but for >30% of fixed nitrogen (N) loss (3–6) due to the onset of anaerobic processes, including denitrification and anammox (7–10). Both field and modeling observations point to the expansion of low oxygen regions as a result of global warming (11). Thus, to evaluate the biogeochemical impact of these regions, it is imperative to understand fully how oxygen controls the cycling of substrates involved in nitrogen loss pathways.

Recent studies have quantified the oxygen sensitivity of anaerobic OMZ nitrogen transformations, finding that denitrification has relatively low oxygen tolerance with a half-inhibition concentration (IC_{50}) of 0.3 μmol·L^{-1}, compared with higher values for nitrate reduction (4 to ≥20 μmol·L^{-1}) and anammox (1 to ~10 μmol·L^{-1} O_2) (12–14). Variability in IC_{50} for nitrate reduction and anammox may result from differences in microbial community composition or the variable presence of aggregates with anoxic microsites (12, 14).

The oxygen kinetics of aerobic nitrification are poorly constrained relative to the oxygen sensitivity for the anaerobic processes. Field studies point to low apparent half-saturation constant (K_m) values in OMZ waters, where, for example, ammonium oxidation rates decreased by ≤50% of maximum rates in N_2 or He purged controls, with oxygen concentrations estimated to be ≤1 μM (12, 15). Similarly, at <1 μmol·L^{-1} O_2, nitrite oxidation rates were 36–59% of the activity observed at >10 μmol·L^{-1} O_2 in the Peruvian and Namibian OMZs (10, 16). Still, the kinetics of these processes have not been explored for oxygen concentrations of less than 0.25 μmol·L^{-1}, and K_m values for oxygen have not been resolved. Ammonium and nitrite oxidation are generally active in incubations of waters from anoxic parts of the OMZ, although these rates are usually low relative to the adjacent oxygen-containing waters (10, 16–18). Recent developments in oxygen detection reveal, however, that even "anoxic" incubations easily suffer from oxygen contamination (18–20).

Significance

As an essential nutrient, nitrogen plays a critical role in regulating oceanic primary productivity. Nitrogen is cycled between bioavailable and nonavailable forms through a network of aerobic and anaerobic microbial processes. Expanding oxygen minimum zones are hot spots for such transformations. Using a highly sensitive oxygen-sensing technique, we demonstrate that two key aerobic processes, ammonium oxidation and nitrite oxidation, persist even at low oxygen levels of 5–30 nM (~0.01% air saturation). Activity at these low oxygen concentrations allows ammonium and nitrite oxidation to persist at oxic/anoxic boundaries and within anoxic waters if oxygen intrudes at sufficient frequency. In such environments, ammonium and nitrite oxidizers compete with anaerobic organisms for ammonium and nitrite, and thus act to control nitrogen loss.

Author contributions: L.A.B., T.D., J.J.W., S.J.H., O.U., D.E.C., N.P.R., and B.T. designed research; L.A.B., T.D., L.T., D.B.M., J.J.W., O.U., D.E.C., and N.P.R. performed research; L.A.B., T.D., L.T., D.B.M., A.D.B., N.P.R., and B.T. analyzed data; and L.A.B. and B.T. wrote the paper.

The authors declare no conflict of interest.

This article is a PNAS Direct Submission.

Data deposition: The sequences reported in this paper have been deposited in the National Center for Biotechnology Information (NCBI) database (accession no. PRJNA335767).

[1]Present address: Biogeochemistry Department, Max Planck Institute for Marine Microbiology, 28359 Bremen, Germany.

[2]To whom correspondence should be addressed. Email: lbristow@mpi-bremen.de.

This article contains supporting information online at www.pnas.org/lookup/suppl/doi:10.1073/pnas.1600359113/-/DCSupplemental.

Oxygen concentrations in the OMZ core generally fall below the detection limit (<1–10 nmol·L^{-1}) of the highly sensitive switchable trace amount oxygen (STOX) sensors (21–25). The nondetectable levels of oxygen in conjunction with the dominance of gene transcripts associated with anaerobic processes (26) and the long residence time of OMZ waters (upward of several months) imply that the OMZ cores are, to a wide extent, functionally anoxic (22, 27). Still, intrusions of oxygen to nanomolar levels are occasionally observed within the OMZ core (22, 23) and could potentially support aerobic ammonium and nitrite oxidation. Indeed, natural abundance isotopic signatures of nitrate and nitrite suggest an important role for nitrite recycling to nitrate within OMZs, particularly at the low oxygen fringes (28). Also, direct competition between aerobic and anaerobic populations at nanomolar oxygen levels has been indicated in the Black Sea chemocline, where anaerobic anammox bacteria appear to outcompete aerobic nitrite oxidizers for nitrite (29). Resolving the oxygen kinetics of these processes at low nanomolar levels is essential to understanding the regulation of N loss in OMZs.

We explored the oxygen kinetics of ammonium and nitrite oxidation, as well as nitrate reduction, over the oxygen concentration range of 5 nmol·L^{-1} to 20 μmol·L^{-1} in waters of the seasonal OMZ off central Chile. Our results demonstrate that all three processes have a strong dependence on nanomolar oxygen concentrations, but also that ammonium and nitrite oxidation can be active and important at the lowest oxygen levels analyzed.

Results and Discussion

In the eastern South Pacific, low oxygen conditions exist between 0° and 37°S (30, 31). Off the coasts of Peru and northern Chile, these conditions persist year round in the permanent OMZ, whereas seasonal oscillations occur at our study site off Concepcion, Chile at 36°S. Here, complete oxygen depletion is only observed during the austral summer (32–34) when upwelling-favorable southerly winds dominate, allowing nutrient-rich, oxygen-depleted equatorial subsurface waters to intrude across the shelf. This advection of nutrients stimulates primary productivity, enhancing organic matter export and thereby generating higher rates of subsurface respiration (34, 35).

Oxygen concentrations during the time of our experiments (March 2012) decreased from near saturation at the surface to below detection between 40 and 50 m, and then remained below the detection limit of the in situ STOX sensor (about 10 nmol·L^{-1}) to the seabed (23) (Fig. 1). With the disappearance of oxygen, nitrite increased from 0.1 μmol·L^{-1} at 40 m to 2.7 μmol·L^{-1} at 85 m, alongside a decrease in nitrate concentrations (Fig. 1), indicative of dissimilatory nitrate reduction to nitrite. Ammonium concentrations peaked at 1.3 μmol·L^{-1} in the upper oxic water column, but remained below 0.4 μmol·L^{-1} in the oxygen-depleted bottom water (Fig. 1).

Oxygen Sensitivity of Ammonium Oxidation. Oxygen sensitivity tests were undertaken with water sampled at the oxygen-depleted depth of 50 m. Ammonium oxidation rates depended strongly on oxygen concentrations in the nanomolar range (Fig. 2). Maximal rates of ~40 nmol·L^{-1} N·d^{-1} were seen at oxygen concentrations above 1 μmol·L^{-1}, and rates declined sharply at lower concentrations. Nonetheless, rates were detectable to the lower limit of our oxygen measurements, with 12% of the maximal activity remaining at an oxygen concentration of 6 nmol·L^{-1} (Fig. 2). These results indicate that ammonium oxidation proceeded at or below the detection limit of the in situ STOX sensor and that rates can be stimulated strongly by the injection of oxygen. Michaelis–Menten kinetics fitted to these data produced an apparent K_m of 333 ± 130 nmol·L^{-1} O_2 (Fig. 2). This oxygen response likely represents the response of a mixed community potentially carrying a variety of terminal oxidases with different K_m values.

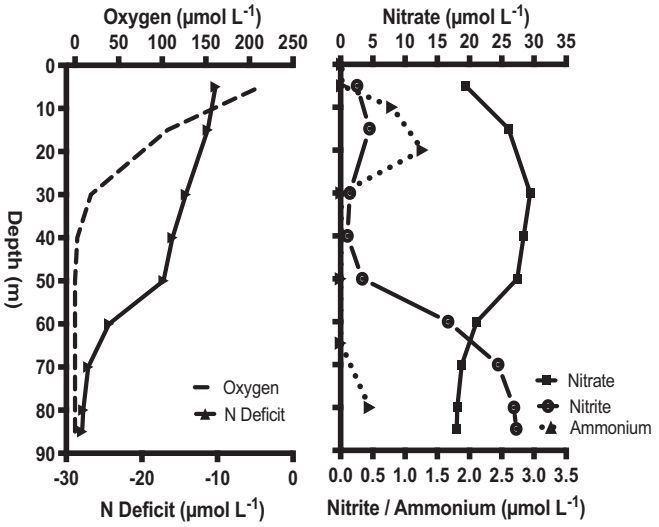

Fig. 1. Depth profiles of hydrochemical parameters from station 18, off Concepcion, Chile. Oxygen concentrations (dashed line) measured with an SBE-43 sensor relative to the N deficit [N deficit = ($[NO_3^-] + [NO_2^-] + [NH_4^+]$) − 16 × $[PO_4^{3-}]$) × 0.86)] (*Left*) and to profiles of nitrate, nitrite, and ammonium (*Right*).

Prior studies at our study site have shown that the ammonium oxidizer community is dominated by Archaea (36), which are abundant and diverse under oxygen-deficient conditions (37). We used small subunit (SSU) ribosomal rRNA gene pyrosequencing with primers encompassing both Bacteria and Archaea to describe microbial population diversity at 50 m. Between 53% and 58% of all sequences were affiliated with four monophyletic clades within the phylum Thaumarchaeota (Fig. S1): *Nitrosopumilus*, *Nitrosopelagicus* water column A, unaffiliated water column B, and marine benthic group B (38–40). The most abundant thaumarchaeal phylotype observed was affiliated with the *Nitrosopumilus* cluster, a group that contains cultivated, ammonium-oxidizing representatives (39) and has been observed in a wide array of marine environments (41, 42). The Thaumarchaeota observed here displayed close relationships to those observed in permanent and seasonally anoxic OMZs and anoxic basins, such as the eastern tropical South Pacific and Saanich Inlet, respectively (43, 44) (Fig. S1). No sequences observed were affiliated with any genus of ammonium-oxidizing bacteria or with *Nitrospira*, which may oxidize both ammonium and nitrite (45). We thus conclude that ammonium oxidation was likely fueled exclusively by Thaumarchaeota, as in other low oxygen regions (17, 46). Cultivated, ammonium-oxidizing *Nitrosopumilus maritimus* strain SCM1 has an apparent K_m for oxygen of 3.9 ± 0.6 μmol·L^{-1} and ceases to grow under oxygen limitation, suggesting a limited capacity to survive under low oxygen conditions (39). Thus, the ammonium-oxidizing Archaea (AOA) community of the OMZ appears to be better adapted to low oxygen than *N. maritimus*. Curiously, the apparent K_m for oxygen for *N. maritimus* is high, considering its COX1-type terminal oxidase (47), with such oxidases typically having K_m values of 0.2 μM (48). Thus, the oxygen kinetics of ammonium oxidation appear not to depend on the terminal oxidase alone, and detailed biochemical and physiological studies would be needed to explore the difference between *N. maritimus* and the OMZ Thamarchaeota further.

Oxygen Sensitivity of Nitrite Oxidation. Similar to ammonium oxidation, nitrite oxidation showed a high affinity for oxygen, with a strong dependence on oxygen in the nanomolar range (Fig. 2). Rates were approximately fivefold higher than the rates for ammonium oxidation, with maximal rates >200 nmol·L^{-1} N·d^{-1} at oxygen concentrations greater than 1.6 μmol·L^{-1}. As oxygen

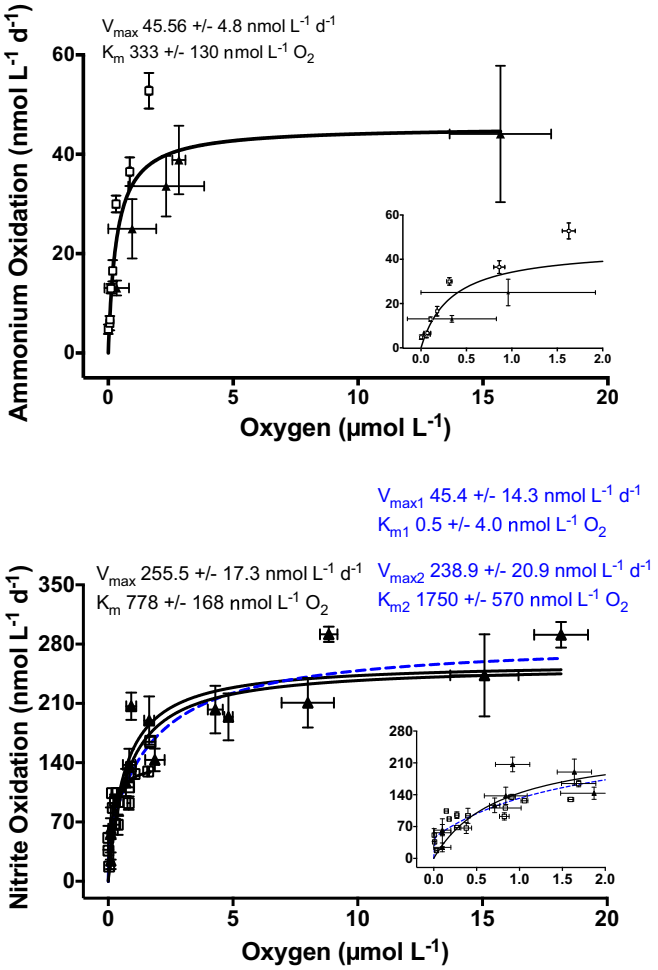

Fig. 2. Ammonium (*Top*) and nitrite (*Bottom*) oxidation rates over experimentally manipulated oxygen conditions (5 nmol·L^{-1} to 20 µmol·L^{-1}). Rates were determined at oxygen concentrations between 5 nmol·L^{-1} and 2 µmol·L^{-1} with continuous monitoring by STOX sensors (□) and 100 nmol·L^{-1} to 20 µmol·L^{-1} using serum bottles (▲). Fitted one-component (solid black line and black text) and two-component (dashed blue line and blue text, for nitrite oxidation only) Michaelis–Menten kinetics allowed the apparent K_m and V_{max} to be calculated (with SEs). (*Insets*) Same data magnified, showing 0–2 µmol·L^{-1} oxygen. Error bars represent the SE.

concentrations declined, nitrite oxidation rates dropped sharply, yet a mean rate of 35 nmol·L^{-1} N·d^{-1} persisted at 5–33 nmol·L^{-1} O_2. Hence, rates of both ammonium and nitrite oxidation were detectable in the low nanomolar range (5–33 nmol·L^{-1} O_2). The response to oxygen was consistent across multiple depths (30, 40, and 50 m), with in situ oxygen conditions ranging from below detection to 19 µmol·L^{-1} and nitrite concentrations in the range of 0.1–0.45 µmol·L^{-1}. A one-component Michaelis–Menten fit to the nitrite oxidation data produced an apparent K_m of 778 ± 168 nmol·L^{-1} O_2 (Fig. 2). Although this result suggests a lower oxygen affinity for nitrite oxidation compared with ammonium oxidation, the fitted Michaelis–Menten kinetics generally underestimated the measured nitrite oxidation rates in the low nanomolar range (<300 nmol·L^{-1}; Fig. 2, *Inset*). This mismatch suggests that the kinetic response has a high-affinity component.

To evaluate this response, we calculated values for a two-component Michealis–Menten model, which gave a significantly better fit to the data (sum of squares F test; $F_{2,26} = 6.2$, $P = 0.0062$). Although the two resulting apparent K_m values are not well constrained ($K_{m1} = 0.5 \pm 4.0$ nmol·L^{-1}; $K_{m2} = 1{,}750 \pm 570$ nmol·L^{-1}), this model fit supports the presence of a high-affinity component, which accounted for ∼15% of the maximum nitrite oxidation rate ($V_{max1} = 45 \pm 14$ nmol·L^{-1}·d^{-1}; $V_{max2} = 239 \pm 21$ nmol·L^{-1}·d^{-1}; Fig. 2). A high-affinity component for nitrite oxidation, and hence nitrite oxidation having a higher affinity for low nanomolar oxygen than that observed for ammonium oxidation, aligns with the typical depth distribution of AOA and nitrite-oxidizing bacteria (NOB) observed in OMZs, where NOB are typically distributed deeper and at higher abundances into the OMZ core relative to AOA (17, 49).

Nitrospina-like bacteria were the only nitrite oxidizers identified in our SSU rRNA gene analysis (Fig. S1), consistent with prior work at our study site (50), and similar to other low oxygen regions (16, 18, 49). This phylogenetic similarity suggests that our observed kinetic response could be consistent across low oxygen systems. Microaerobic adaptations have been identified in the genome of a marine *Nitrospina gracilis* strain, including the presence of a putatively high-affinity *cbb*$_3$-type terminal oxidase (51). A K_m value of 7 nmol·L^{-1} O_2 was previously determined for a *cbb*$_3$-type oxidase (52) broadly consistent with the high-affinity component inferred here. The *cbb*$_3$-type oxidase was the only terminal oxidase robustly identified in the *N. gracilis* genome. An additional cytochrome *bd* terminal oxidase, which typically has a lower oxygen affinity, was also identified, but it was not thought to be involved in oxygen respiration, because residues responsible for quinol binding were lacking (51). Physiological variability across the *Nitrospina* clade has to be expected, however, and because low-affinity oxidases are generally more efficient in energy conservation (53), the possession of an additional functional terminal oxidase with lower oxygen affinity, as suggested by our results, would constitute metabolic versatility. Similar to the ammonium oxidizers, detailed studies of other *Nitrospina* strains are required to link the community's oxygen response to cell physiology.

Anaerobic nitrite oxidation is known to occur as part of the anammox metabolism, with nitrite acting as an electron donor during carbon fixation; hence, growth is associated with nitrate production (54). However, during our study, anammox activity was only detected at 80 m, at a rate of 2 nmol·L^{-1} N·d^{-1}, and the process was also previously only observed close to the sediment–water interface at this site (33, 55). Hence, we do not expect anammox to contribute significantly to total nitrite oxidation here. We note also that it would be thermodynamically feasible for NOB to use an alternate electron acceptor to oxygen, such as iodate (56), allowing the process to proceed in anaerobic conditions. The occurrence of such a process in marine systems has yet to be demonstrated. However, the high oxygen affinity demonstrated here implies that NOB in OMZs perform aerobic nitrite oxidation even below the lowest in situ detection limit for oxygen achieved so far (21).

Oxygen Sensitivity of Nitrate Reduction. The exceptionally high oxygen affinities of ammonium and nitrite oxidizers reinforce the possibility that these organisms coexist with anaerobes. Such overlaps between N-cycling processes have implications for the turnover, retention, and substrate supply within an OMZ. For example, when nitrite is cycled between nitrite oxidation and dissimilatory nitrate reduction, N is retained in the system (28). Nitrate reduction has been shown to be the least oxygen-sensitive of the anaerobic pathways, with activity observed up to 25 µmol·L^{-1} O_2 (12, 15). Therefore, a large overlap could occur between nitrate reduction and ammonium and nitrite oxidation. In the present study, however, nitrate reduction from the oxygen-depleted depth of 50 m was highly sensitive to nanomolar oxygen concentrations, with an IC_{50} of 0.73 ± 0.5 µmol·L^{-1} O_2 (Fig. 3) and a maximum rate of 197 ± 26 nmol·L^{-1} N·d^{-1}. Complete inhibition was observed above 6 µmol·L^{-1} O_2. Potential explanations for the difference from previous studies include possible differences in the populations of nitrate reducers, which generally exhibit high

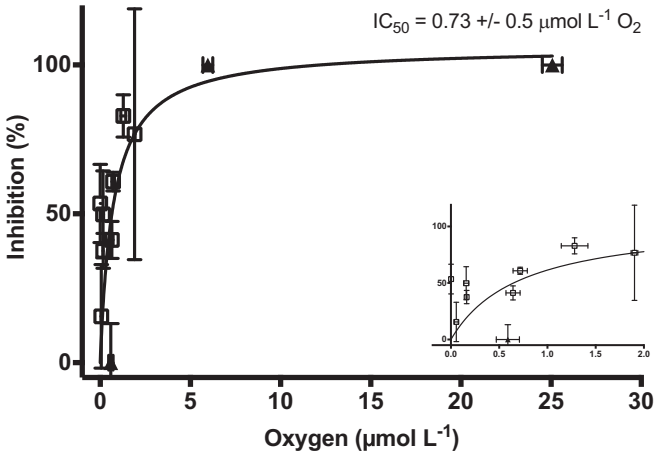

Fig. 3. Inhibition of nitrate reduction by oxygen, where oxygen was manipulated between 5 nmol·L^{-1} and 25 µmol·L^{-1}, with water sampled from a depth of 50 m. Inhibition was determined by the difference between the maximum rate observed and zero (undetectable rate) representing complete inhibition. Experiments carried out in a setup with continuous monitoring by STOX sensors (□) and experiments carried out in serum bottles (▲) are shown. Error bars represent the SE.

phylogenetic diversity (26, 46, 57), and differences in the particle size distributions, because larger aggregates may hold oxygen-depleted microniches (12, 58). The latter effect was specifically suggested to explain lower oxygen sensitivity of anammox at coastal, presumably more particle-rich, sites than at offshore OMZ sites (12), but our results demonstrate that the oxygen sensitivity can also be high in coastal waters. Our results also indicate that the previously suggested potential for nitrate reduction to nitrite to initiate N cycling at micromolar oxygen concentrations cannot be generalized across OMZ environments.

Implications. Here, we present detailed determinations of oxygen kinetics and apparent K_m values for ammonium and nitrite oxidation over environmentally relevant oxygen concentrations for an OMZ. As highlighted above, the AOA and NOB communities at our study site are similar to the AOA and NOB communities observed in the permanent, open ocean OMZs, suggesting that the kinetics determined here are applicable across OMZ systems. Combining our data with data from previous oxygen sensitivity studies in the Peruvian and Namibian OMZs that did not reach as low oxygen concentrations (10, 12, 16) lends further support to the generalization of our results and also illustrates the gap, which has now been filled (Fig. S2; rates from all studies were normalized to maximal rates, because the apparent V_{max} varies as a result of variability in cell numbers, whereas the apparent K_m will not be influenced). For ammonium oxidation, the lack of any clear oxygen dependence in the previous results obtained at oxygen concentrations ≥0.6 µmol·L^{-1} is consistent with the apparent K_m of 0.3 µmol·L^{-1} found here. In the case of nitrite oxidation, the general tendency of the previously measured rates to increase from the lowest studied oxygen concentrations of 0.25 µmol·L^{-1} is also consistent with the kinetic response that is resolved well by our data. Accordingly, apparent K_m values for both processes from the combined datasets are within error of those K_m values obtained in this study. These kinetics indicate, on the one hand, that ammonium and nitrite oxidation function under nanomolar oxygen concentrations with rates highly dependent on the actual oxygen level and, on the other hand, that these processes are strongly suppressed under anoxia.

Further comparison of our low K_m values for ammonium and nitrite oxidation, alongside the IC_{50} value for anammox, denitrification, and nitrate reduction (this study and refs. 12 and 14), indicates that the potential for overlap between aerobic and anaerobic processes varies strongly by location, due to the large variation in IC_{50}. Thus, with IC_{50} values less than 1 µmol·L^{-1} for the anaerobic processes (this study and ref. 14), overlap is largely restricted to the nanomolar range, in contrast to the low micromolar range based on the results of Kalvelage et al. (12). Further experimental analysis of the factors (as discussed above) causing the large variability in IC_{50} within and among studies is needed. However, considering that nitrite oxidation rates approach saturation already at ∼1 µmol·L^{-1} O_2 (Fig. 2*B*) and that the rates in the lower oxycline are generally high compared with anammox and denitrification rates (e.g., 10, 18), it is evident that this process provides strong competition for available nitrite even in settings where the anaerobic processes have a high oxygen tolerance.

We observed active ammonium and nitrite oxidation to the lowest oxygen levels analyzed (Fig. 2), with nitrite oxidation maintaining a particularly high relative activity at oxygen levels corresponding to the typical detection limit for in situ STOX oxygen measurements (∼10 nmol·L^{-1}) (18, 22, 23, 59). These observations imply that the processes could be active in the apparently oxygen-depleted OMZ core provided that oxygen is supplied at a sufficient rate. Such may be the case at the fringes of the OMZs, where intrusions of nanomolar oxygen levels are occasionally observed (22, 23). Thus, nanoaerobic nitrite oxidation may explain the recycling of nitrate inferred from nitrogen and oxygen isotope patterns observed there (28). Under these conditions, ammonium and nitrite oxidation would be able to compete for substrates critical to the N loss processes of anammox and denitrification, hence affecting total N loss in these systems. The oxygen kinetics determined here should therefore be incorporated into models not only to assess the role of nitrite and how it is produced and lost within OMZ systems but also, more importantly, to understand N cycling with the predicted expansion of low oxygen waters throughout the global ocean.

Materials and Methods

Samples were collected during the MOOMZ 4 cruise (Microbial Oceanography of Oxygen Minimum Zones cruise no. 4 onboard *R/V Kay Kay II*; March 20–26, 2012) at the COPAS (Centro de Investigación Oceanográphica en el Pacífico Sur-Oriental) time series site, station 18, off the coast of Concepcion, Chile (36°30′85 S, 73°07′75 W). Station 18 is located 18 nautical miles offshore, with a total water depth of ∼93 m. Water was sampled using a pump profiling system (PPS) (24) equipped with a SeaBird SBE 25 CTD (conductivity, temperature, and depth measuring device), SBE 43 oxygen sensor, and in situ STOX unit (23).

High-resolution oxygen profiling was carried out initially alongside nutrient determinations to characterize the water column and determine depth selection for oxygen sensitivity experiments. Tiano et al. (23) discussed the oxygen depth profiles from across the sampling period with particular focus on the submicromolar range. Nitrate, nitrite, and phosphate concentrations were measured at a land-based laboratory using standard protocols (60). Ammonium concentrations were determined fluorometrically by the orthophthaldialdehyde method (61). The N deficit was calculated as follows, $([NO_3^-] + NO_2^- + NH_4^+] - 16 \times [PO_4^{3-}]) \times 0.86$, with 0.86 used to take into account the release of PO_4^{3-} from organic matter remineralized during denitrification (5).

Samples were taken for the determination of anammox and denitrification rates from five depths between the oxycline and sediment water interface, following sampling and experimental procedures outlined by Dalsgaard et al. (9). Two amendments were made at each depth, 5 µM $^{15}NH_4^+$ and 5 µM $^{15}NO_2^-$, with triplicate exetainers killed at 0 and 12 h. Analysis and calculations followed the principles outlined by Dalsgaard et al. (9).

Oxygen Sensitivity Experiments (5 nmol·L^{-1} to 2 µmol·L^{-1} O_2). Seawater was sampled from 40 and 50 m (representing the oxycline and OMZ core) directly from the PPS into a 20-L glass bottle. The bottle was overflowed (at least three volume equivalents), flushing the bottle before filling and the headspace while filling with N_2 gas, and sealed without bubbles using deoxygenated butyl rubber stoppers (19, 59). On return to the land-based laboratory, the bottle was degassed with helium (∼40 min) and was spiked with one of three amendments: 2 µmol·L^{-1} $^{15}NH_4^+$ + 2 µmol·L^{-1} $^{14}NO_2^-$ to measure ammonium oxidation (only done at 50 m), 2 µmol·L^{-1} $^{15}NO_2^-$ + 2 µmol·L^{-1} $^{14}NO_3^-$ to measure nitrite oxidation, or 10 µmol·L^{-1} $^{15}NO_3^-$ + 5 µmol·L^{-1} $^{14}NO_2^-$

to measure dissimilatory nitrate reduction to nitrite (only done at 50 m). The addition of ^{14}N compounds served to trap ^{15}N-labeled products. The water was then dispensed into custom-modified SCHOTT DURAN glass bottles (1,160 mL) (62), eight bottles per depth per treatment. An additional modification was the placement of a third glass port on the bottle, which held a 100-mL glass reservoir filled with sample water, that was continually degassed with helium for the duration of the experiment. During the incubations, the bottles were continuously stirred with a glass-coated magnetic stir bar (62), kept in the dark, and submersed in a water bath to maintain in situ temperature. Oxygen additions were made to the bottles by injecting known volumes of air-saturated seawater; two bottles per depth per treatment received no oxygen addition. In this setup, oxygen was monitored throughout the incubations with a STOX sensor in each bottle. Time-series sampling was undertaken at 0, 3, 6, 9, and 12 h by inserting a long needle down the pressure compensation tube, opening the valve to the reservoir, allowing the reservoir water to flow into the incubation vessel, and replacing the 10 mL of sample that was withdrawn. Samples were filtered through a 0.22-μm cellulose acetate filter and frozen until analysis.

Oxygen Sensitivity Experiments (100 nmol·L^{-1} to 20 μmol·L^{-1} O_2). Seawater was sampled from 30, 40, and 50 m representing different in situ oxygen conditions. Water was sampled directly from the PPS into 120-mL serum bottles, allowing water to overflow for approximately three volume changes before sealing (without bubbles) with deoxygenated butyl rubber stoppers (19). Bottles were stored in the dark until the start of the experiment (always <12 h). Serum bottles were amended with ^{15}N-labeled substrates. The same three ^{15}N amendments as mentioned above were carried out; $^{15}NO_2^-$ at all depths and $^{15}NH_4^+$ and $^{15}NO_3^-$ at 50 m only. For each amendment, four serum bottles were spiked with ^{15}N substrate. Saturated $HgCl_2$ (200 μL) was immediately added to one bottle, which served as a "killed" control. A volume of 20 mL was subsequently removed from all bottles to create a headspace, which was then flushed twice with helium. The removed 20 mL was filtered through a 0.22-μm cellulose acetate filter and frozen for "time zero" analysis. Injections of air or pure oxygen were then made into the headspace to manipulate oxygen concentrations with oxygen solubility determined using the equation provided by Garcia and Gordon (63). A subset of the amendments received no oxygen injection (100 nmol·L^{-1} on average). After 6, 12, and 24 h, an additional 15 mL was removed, filtered, and frozen. After removing the sample at 6 and 12 h, headspaces were flushed twice with helium and oxygen additions were made again. After 24 h, oxygen concentrations in the serum bottles were determined using a Clark-type oxygen electrode (64).

Rate Determination. Nitrite oxidation rates were determined based on $^{15}NO_3^-$ production in incubations with $^{15}NO_2^-$. After removal of any unused $^{15}NO_2^-$ from the initial amendment using sulfamic acid, $^{15}NO_3^-$ was converted to $^{15}NO_2^-$ with cadmium and then to N_2 with sulfamic acid (16, 65). Ammonium oxidation and nitrate reduction rates were determined based on $^{15}NO_2^-$ production in incubations with $^{15}NH_4^+$ or $^{15}NO_3^-$. The $^{15}NO_2^-$ produced during incubations was converted to N_2 with sulfamic acid (16). The N_2 produced ($^{14}N^{15}N$ and $^{15}N^{15}N$) was analyzed on a gas chromatography isotope ratio mass spectrometer as described by Dalsgaard et al. (9). Rates for all processes were evaluated from the slope of the linear regression of ^{15}N production with time, and corrected for the fraction of the N pool labeled in the initial substrate pool. A *t* test was applied to determine if rates were significantly different from zero ($P < 0.05$). Detection limits for the oxygen sensitivity experiments were estimated from the median of the SE of the slope, multiplied by the *t* value for $P = 0.05$. Thus, detection limits were 4.8 nmol·L^{-1} N·d^{-1} for ammonium oxidation, 28.8 nmol·L^{-1} N·d^{-1} for nitrite oxidation, and 28.8 nmol·L^{-1} N·d^{-1} for nitrate reduction.

The parameters V_{max} and K_m for Michaelis–Menten kinetics were derived from the rate data by nonlinear least squares fits of either single [rate = V_{max} * $[O_2]/(K_m + [O_2])$] or double [rate = V_{max1} * $[O_2]/(K_{m1} + [O_2])$ + V_{max2} * $[O_2]/(K_{m2} + [O_2])$] rate expressions. The fits were made in GraphPad Prism based on the Levenberg–Marquardt algorithm.

SSU Ribosomal RNA Gene Sequencing. Approximately 20 L of GFA (glass fiber filter; 1.6 μm)-prefiltered seawater spanning four depth intervals collected at 5, 29, 50, and 85 m was passed through 0.2-μm Serivex filters (10 L per filter for each depth interval) using previously reported sample collection and filtration protocols. These protocols can be viewed as visualized experiments at www.jove.com/video/1159/ (66) and www.jove.com/video/1161/ (67), respectively. DNA was extracted from Sterivex filters as described by Zaikova et al. (66) and DeLong et al. (68). The DNA extraction protocol can be viewed as a visualized experiment at www.jove.com/video/1352/ (69). DNA extracts from the 50-m depth interval were amplified using the universal three domain primers 926F (5′-cct atc ccc tgt gtg cct tgg cag tct cag AAA CTY AAA KGA ATT GRC GG-3′) and 1392R (5′-cca tct cat ccc tgc gtg tct ccg act cag-<XXXXX>-ACG GGC GGT GTG TRC-3′) targeting the V6–V8 region of the SSU ribosomal RNA (16S rRNA) gene. Primer sequences were modified by the addition of 454 A or B adapter sequences (lowercase). In addition, the reverse primer included a 5-bp barcode designated <XXXXX> for multiplexing of samples during sequencing. Twenty-microliter PCR reactions were performed in duplicate and pooled to minimize PCR bias using 0.4 μL of Advantage GC 2 Polymerase Mix (Advantage-2 GC PCR Kit; Clontech), 4 μL of 5X GC PCR buffer, 2 μL of 5M GC Melt Solution, 0.4 μL of 10 mM dNTP mix (MBI Fermentas), 1.0 μL of each 25 nM primer, and 10 ng of sample DNA. The thermal cycler protocol was 95 °C for 3 min; 25 cycles of 95 °C for 30 s, 50 °C for 45 s, and 68 °C for 90 s; and a final 10-min extension at 68 °C. PCR amplicons were purified using SPRI Beads and quantified using a Qubit fluorometer (Invitrogen). Samples were diluted to 10 ng/μL and mixed in equal concentrations. Emulsion PCR and sequencing of the PCR amplicons were performed at the Department of Energy Joint Genome Institute following the Roche 454 GS FLX Titanium (454 Life Sciences) technology according to the manufacturer's instructions.

Pyrotag Sequence Processing and Phylogenetic Analysis. Pyrotag sequences from three independent runs of the 50-m sample were pooled, trimmed to a fixed length (250 nt), and analyzed using the "UPARSE" pipeline in USEARCH (version 6.0) (70). Briefly, samples were dereplicated (USEARCH command "derep_fulllength"), sorted by size (USEARCH command "sortbysize," minsize option 2 to exclude singletons), and clustered in operational taxonomic units at 97% nucleotide identity (command -cluster_otus). OTU sequences were then screened for chimeras against the SILVA rRNA gene database (version 119, command "uchime_ref"). Dereplicated sequences were then mapped to OTU sequences (command "usearch_global"). Nonchimeric OTU sequences were directly compared with the SILVA rRNA database (version 119) and 16S rRNA genes from the eastern tropical South Pacific and Saanich Inlet using the nucleotide basic local alignment search tool (BLASTN) (71). Relative abundance matrices were generated based on the best-BLAST hit to the SILVA rRNA gene database using the "summarize_taxa.py" script in the QIIME software package (72). Thaumarchaeal 16S rRNA genes, their respective best-BLASTN hits, and pure-culture thaumarchaeal rRNAs were aligned using the SINA alignment tool with the default settings. The resulting alignment was then imported into the ARB environment. Phylogenetic trees of partial full-length 16S rRNA genes (600 bp or greater) were made using neighbor-joining with the jukes-cantor correction. Short sequences were then inserted into this backbone tree using the parsimony tool.

ACKNOWLEDGMENTS. We thank the crew of the *R/V Kay Kay II* for their help in sample collection, Gadiel Alarcón for his help with the PPS, Joe Jennings and Montserrat Aldunate for nutrient analysis, Lars Borregaard Pedersen and Preben Sørensen for making STOX sensors, and Christian Kondrup for constructing glassware. We thank the editor and two anonymous reviewers for their comments and thoughtful suggestions. This study was supported by the Danish National Research Foundation (Grant DNRF53), the Danish Council of Independent Research, European Research Council ("Oxygen" Grant 267233), and the Agouron Institute. T.D. acknowledges support from the Arctic Research Centre, Aarhus University. A.D.B. and O.U. were supported by the Millennium Scientific Initiative (Grant IC 120019) and the Chilean National Commission for Scientific and Technological Research (Grant Fondecyt 3160611). S.J.H. was supported by the G. Unger Vetlesen and Ambrose Monell Foundations, the Tula Foundation-funded Centre for Microbial Diversity and Evolution, the Natural Sciences and Engineering Research Council of Canada, Genome British Columbia, the Canada Foundation for Innovation, and the Canadian Institute for Advanced Research.

1. Falkowski PG, Fenchel T, Delong EF (2008) The microbial engines that drive Earth's biogeochemical cycles. *Science* 320(5879):1034–1039.
2. Wyrtki K (1962) The oxygen minima in relation to ocean circulation. *Deep Sea Res* 9: 11–23.
3. Karstensen J, Stramma L, Visbeck M (2008) Oxygen minimum zones in the eastern tropical Atlantic and Pacific oceans. *Prog Oceanogr* 77(4):331–350.
4. Gruber N, Sarimento JL (1997) Global patterns of marine nitrogen fixation and denitrification. *Global Biogeochem Cycles* 11:235–266.
5. Codispoti LA, et al. (2001) The oceanic fixed nitrogen and nitrous oxide budgets: Moving targets as we enter the anthropocene. *Scientia Marina* 65:85–102.
6. DeVries T, Deutsch C, Rafter PA, Primeau F (2013) Marine denitrification rates determined from a global 3-D inverse model. *Biogeosciences* 10:2481–2496.

7. Kuypers MM, et al. (2005) Massive nitrogen loss from the Benguela upwelling system through anaerobic ammonium oxidation. *Proc Natl Acad Sci USA* 102(18):6478–6483.
8. Thamdrup B, et al. (2006) Anaerobic ammonium oxidation in the oxygen-deficient waters off northern Chile. *Limnol Oceanogr* 51:2145–2156.
9. Dalsgaard T, Thamdrup B, Farías L, Revsbech NP (2012) Anammox and denitrification in the oxygen minimum zone of the eastern South Pacific. *Limnol Oceanogr* 57: 1331–1346.
10. Kalvelage T, et al. (2013) Nitrogen cycling driven by organic matter export in the South Pacific oxygen minimum zone. *Nat Geosci* 6:228–234.
11. Stramma L, Johnson GC, Sprintall J, Mohrholz V (2008) Expanding oxygen-minimum zones in the tropical oceans. *Science* 320(5876):655–658.
12. Kalvelage T, et al. (2011) Oxygen sensitivity of anammox and coupled N-cycle processes in oxygen minimum zones. *PLoS One* 6(12):e29299.
13. Jensen MM, Kuypers MMM, Lavik G, Thamdrup B (2008) Rates and regulation of anaerobic ammonium oxidation and denitrification in the Black Sea. *Limnol Oceanogr* 53:23–36.
14. Dalsgaard T, et al. (2014) Oxygen at nanomolar levels reversibly suppresses process rates and gene expression in anammox and denitrification in the oxygen minimum zone off northern Chile. *MBio* 5(6):e01966.
15. Lipschultz F, et al. (1990) Bacterial transformations of inorganic nitrogen in the oxygen-deficient waters of the Eastern Tropical South Pacific Ocean. *Deep Sea Res A* 37: 1513–1541.
16. Füssel J, et al. (2012) Nitrite oxidation in the Namibian oxygen minimum zone. *ISME J* 6(6):1200–1209.
17. Beman JM, Popp BN, Alford SE (2012) Quantification of ammonia oxidation rates and ammonia-oxidizing archaea and bacteria at high resolution in the Gulf of California and eastern tropical North Pacific Ocean. *Limnol Oceanogr* 57:711–726.
18. Ganesh S, et al. (2015) Size-fraction partitioning of community gene transcription and nitrogen metabolism in a marine oxygen minimum zone. *ISME J* 9(12):2682–2696.
19. De Brabandere L, Thamdrup B, Revsbech NP, Foadi R (2012) A critical assessment of the occurrence and extend of oxygen contamination during anaerobic incubations utilizing commercially available vials. *J Microbiol Methods* 88(1):147–154.
20. Lehner P, et al. (2015) LUMOS–A sensitive and reliable optode system for measuring dissolved oxygen in the nanomolar range. *PLoS One* 10(6):e0128125.
21. Revsbech NP, et al. (2009) Determination of ultra-low oxygen concentrations in oxygen minimum zones by the STOX sensor. *Limnol Oceanogr Methods* 7:371–381.
22. Thamdrup B, Dalsgaard T, Revsbech NP (2012) Widespread functional anoxia in the oxygen minimum zone of the eastern South Pacific. *Deep Sea Res Part I Oceanogr Res Pap* 65:36–45.
23. Tiano L, et al. (2014) Oxygen distribution and aerobic respiration in the north and south eastern tropical Pacific oxygen minimum zones. *Deep Sea Res Part 1 Oceanogr Res Pap* 94:173–183.
24. Canfield DE, et al. (2010) A cryptic sulfur cycle in oxygen-minimum-zone waters off the Chilean coast. *Science* 330(6009):1375–1378.
25. Murillo AA, Ramírez-Flandes S, DeLong EF, Ulloa O (2014) Enhanced metabolic versatility of planktonic sulfur-oxidizing γ-proteobacteria in an oxygen-deficient coastal ecosystem. *Front Mar Sci* 1:18.
26. Stewart FJ, et al. (2012) Experimental incubations elicit profound changes in community transcription in OMZ bacterioplankton. *PLoS One* 7(5):e37118.
27. Ulloa O, Canfield DE, DeLong EF, Letelier RM, Stewart FJ (2012) Microbial oceanography of anoxic oxygen minimum zones. *Proc Natl Acad Sci USA* 109(40):15996–16003.
28. Casciotti KL, Buchwald C, McIlvin M (2013) Implications of nitrate and nitrite isotopic measurements for the mechanisms of nitrogen cycling in the Peru oxygen deficient zone. *Deep Sea Res Part I Oceanogr Res Pap* 80:78–93.
29. Lam P, et al. (2007) Linking crenarchaeal and bacterial nitrification to anammox in the Black Sea. *Proc Natl Acad Sci USA* 104(17):7104–7109.
30. Silva N, Rojas N, Fedele A (2009) Water masses in the Humboldt Current System: properties, distribution, and the nitrate deficit as a chemical water mass tracer for Equatorial Subsurface Water off Chile. *Deep Sea Res Part II Top Stud Oceanogr* 56: 992–1008.
31. Cornejo M, Farías L (2012) Following the N_2O consumption in the oxygen minimum zone of the eastern South Pacific. *Biogeosciences* 9:3205–3212.
32. Schulz HN, Strotmann B, Gallardo VA, Jørgensen BB (2000) Population study of the filamentous sulfur bacteria *Thioploca* spp. off the Bay of Concepcion, Chile. *Mar Ecol Prog Ser* 200:117–126.
33. Galán A, Molina V, Belmar L, Ulloa O (2012) Temporal variability and phylogenetic characterization of planktonic anammox bacteria in the coastal upwellng ecosystem off central Chile. *Prog Oceanogr* 92-95:110–120.
34. Montero P, et al. (2007) Productivity cycles in the upwelling area off Concepcion: The importance of diatoms and bacterioplankton in the organic carbon flux. *Prog Oceanogr* 75:518–530.
35. Sobarzo M, Bravo L, Donoso D, Garces-Vargas J, Schneider W (2007) Coastal upwelling and seasonal cycles that influence the water column over the continental shelf off central Chile. *Prog Oceanogr* 75:363–382.
36. Farías L, Fernandez C, Faundez J, Cornejo M, Aleaman ME (2009) Chemolithoautotrophic production mediating the cycling of the greenhouse gases N_2O and CH_4 in an upwelling ecosystem. *Biogeosciences* 6:3053–3069.
37. Molina V, Belmar L, Ulloa O (2010) High diversity of ammonia-oxidizing archaea in permanent and seasonal oxygen-deficient waters of the eastern South Pacific. *Environ Microbiol* 12(9):2450–2465.
38. Francis CA, Roberts KJ, Beman JM, Santoro AE, Oakley BB (2005) Ubiquity and diversity of ammonia-oxidizing archaea in water columns and sediments of the ocean. *Proc Natl Acad Sci USA* 102(41):14683–14688.
39. Martens-Habbena W, Berube PM, Urakawa H, de la Torre JR, Stahl DA (2009) Ammonia oxidation kinetics determine niche separation of nitrifying Archaea and Bacteria. *Nature* 461(7266):976–979.
40. Santoro AE, et al. (2015) Genomic and proteomic characterization of "Candidatus Nitrosopelagicus brevis": An ammonia-oxidizing archaeon from the open ocean. *Proc Natl Acad Sci USA* 112(4):1173–1178.
41. Kamanda Ngugi D, et al. (2015) Comparative genomics reveals adaptations of a halotolerant thaumarchaeon in the interfaces of brine pools in the Red Sea. *ISME J* 9(2):396–411.
42. Nunoura T, et al. (2015) Hadal biosphere: Insight into the microbial ecosystem in the deepest ocean on Earth. *Proc Natl Acad Sci USA* 112(11):E1230–E1236.
43. Zaikova E, et al. (2010) Microbial community dynamics in a seasonally anoxic fjord: Saanich Inlet, British Columbia. *Environ Microbiol* 12(1):172–191.
44. Belmar L, Molina V, Ulloa O (2011) Abundance and phylogenetic identity of archaeoplankton in the permanent oxygen minimum zone of the eastern tropical South Pacific. *FEMS Microbiol Ecol* 78(2):314–326.
45. Daims H, et al. (2015) Complete nitrification by *Nitrospira* bacteria. *Nature* 528(7583): 504–509.
46. Lam P, et al. (2009) Revising the nitrogen cycle in the Peruvian oxygen minimum zone. *Proc Natl Acad Sci USA* 106(12):4752–4757.
47. Walker CB, et al. (2010) *Nitrosopumilus maritimus* genome reveals unique mechanisms for nitrification and autotrophy in globally distributed marine crenarchaea. *Proc Natl Acad Sci USA* 107(19):8818–8823.
48. Rice CW, Hempfling WP (1978) Oxygen-limited continuous culture and respiratory energy conservation in *Escherichia coli*. *J Bacteriol* 134(1):115–124.
49. Beman JM, Leilei Shih J, Popp BN (2013) Nitrite oxidation in the upper water column and oxygen minimum zone of the eastern tropical North Pacific Ocean. *ISME J* 7(11): 2192–2205.
50. Levipan HA, Molina V, Fernandez C (2014) *Nitrospina*-like bacteria are the main drivers of nitrite oxidation in the seasonal upwelling area of the Eastern South Pacific (Central Chile ~36°S). *Environ Microbiol Rep* 6(6):565–573.
51. Lücker S, Nowka B, Rattei T, Spieck E, Daims H (2013) The genome of Nitrospina gracilis illuminates the metabolism and evolution of the major marine nitrite oxidizer. *Front Microbiol* 4:27.
52. Preisig O, Zufferey R, Thöny-Meyer L, Appleby CA, Hennecke H (1996) A high-affinity cbb3-type cytochrome oxidase terminates the symbiosis-specific respiratory chain of Bradyrhizobium japonicum. *J Bacteriol* 178(6):1532–1538.
53. Han H, et al. (2011) Adaptation of aerobic respiration to low O_2 environments. *Proc Natl Acad Sci USA* 108(34):14109–14114.
54. Kartal B, et al. (2013) How to make a living from anaerobic ammonium oxidation. *FEMS Microbiol Rev* 37(3):428–461.
55. Galán A, Faúndez J, Thamdrup B, Santibáñez JF, Farías L (2014) Temporal dynamics of nitrogen loss in the coastal upwelling ecosystem off central Chile: Evidence of autotrophic denitrification through sulfide oxidation. *Limnol Oceanogr* 59(6):1865–1878.
56. Casciotti KL, Buchwald C (2012) Insights on the marine microbial nitrogen cycle from isotopic approaches to nitrification. *Front Microbiol* 3:356.
57. Zumft WG (1997) Cell biology and molecular basis of denitrification. *Microbiol Mol Biol Rev* 61(4):533–616.
58. Kalvelage T, et al. (2015) Aerobic microbial respiration in oceanic oxygen minimum zones. *PLoS One* 10(7):e0133526.
59. De Brabandere L, et al. (2014) Vertical partitioning of nitrogen-loss processes across the oxic-anoxic interface of an oceanic oxygen minimum zone. *Environ Microbiol* 16(10):3041–3054.
60. Grasshoff K, Ehrhardt M, Kremling K, Almgren T (1983) *Methods of Seawater Analysis* (Verlag Chemie, Weinheim, Germany), 2nd revision and extended edition.
61. Holmes RM, Aminot A, Kérouel R, Hooker BA, Peterson BJ (1999) A simple and precise method for measuring ammonium in marine and freshwater ecosystems. *Can J Fish Aquat Sci* 56:1801–1808.
62. Tiano L, Garcia-Robledo E, Revsbech NP (2014) A new highly sensitive method to assess respiration rates and kinetics of natural planktonic communities by use of the switchable trace oxygen sensor and reduced oxygen concentrations. *PLoS One* 9(8): e105399.
63. Garcia HE, Gordon LI (1992) Oxygen solubility in seawater better fitting equations. *Limnol Oceanogr* 37(6):1307–1312.
64. Revsbech NP (1989) An oxygen microelectrode with a guard cathode. *Limnol Oceanogr* 34:472–476.
65. McIlvin MR, Altabet MA (2005) Chemical conversion of nitrate and nitrite to nitrous oxide for nitrogen and oxygen isotopic analysis in freshwater and seawater. *Anal Chem* 77(17):5589–5595.
66. Zaikova E, Hawley A, Walsh DA, Hallam SJ (2009) Seawater sampling and collection. *J Vis Exp* 28:e1159.
67. Walsh DA, Zaikova E, Hallam SJ (2009) Large volume (20L+) filtration of coastal seawater samples. *J Vis Exp* 28:e1161.
68. DeLong EF, et al. (2006) Community genomics among stratified microbial assemblages in the ocean's interior. *Science* 311(5760):496–503.
69. Wright JJ, Lee S, Zaikova E, Walsh DA, Hallam SJ (2009) DNA extraction from 0.22 μM Sterivex filters and cesium chloride density gradient centrifugation. *J Vis Exp* (31): e1352.
70. Edgar RC (2010) Search and clustering orders of magnitude faster than BLAST. *Bioinformatics* 26(19):2460–2461.
71. Altschul SF, Gish W, Miller W, Myers EW, Lipman DJ (1990) Basic local alignment search tool. *J Mol Biol* 215(3):403–410.
72. Caporaso JG, et al. (2010) QIIME allows analysis of high-throughput community sequencing data. *Nat Methods* 7(5):335–336.